

Assignment of Resonance Raman Spectrum of Photoactive Yellow Protein in Its Long-Lived Blue-Shifted Intermediate

Masashi Unno,^{*,†} Masato Kumauchi,[‡] Jun Sasaki,[‡] Fumio Tokunaga,[‡] and Seigo Yamauchi^{*,†}

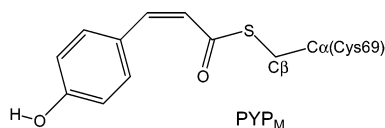
Institute of Multidisciplinary Research for Advanced Materials, Tohoku University, Sendai 980-8577, Japan, and Department of Earth and Space Science, Graduate School of Science, Osaka University, Toyonaka, Osaka 560-0043, Japan

Received: July 3, 2002; In Final Form: November 15, 2002

Photoactive yellow protein (PYP) is a bacterial photoreceptor containing a 4-hydroxycinnamyl chromophore. We report the resonance Raman spectra for the long-lived blue-shifted intermediate of PYP whose chromophore is isotopically labeled with ¹³C at the carbonyl carbon atom or at the ring carbon atoms. Spectra have been also measured with PYP in D₂O where the phenolic hydroxyl group of the chromophore is deuterated. All of the observed Raman bands are assigned on the basis of the observed isotope shifts and normal mode calculations using a density functional theory. The complete assignment provides a satisfactory framework for future investigations of the photocycle mechanism in PYP by vibrational spectroscopy.

Introduction

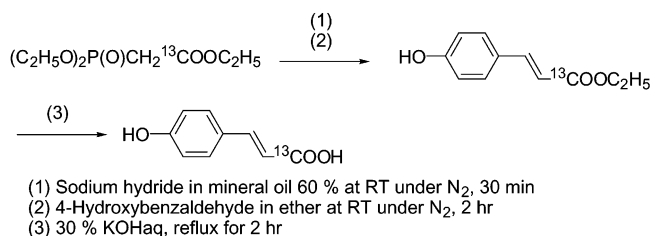
The photoactive yellow protein (PYP) from phototrophic bacterium *Ectothiorhodospira halophila* is a small water-soluble photoreceptor protein,¹ and it has been an attractive model for studying protein structures and dynamics. This protein has the 4-hydroxycinnamyl chromophore, which is covalently linked to Cys69 through a thiolester bond.^{2,3} Photoexcitation of PYP triggers a photocycle that involves several intermediate states.^{4–7} A long-lived blue-shifted intermediate denoted PYP_M (also called I₂ or pB) is the putative signaling state of this photoreceptor protein.



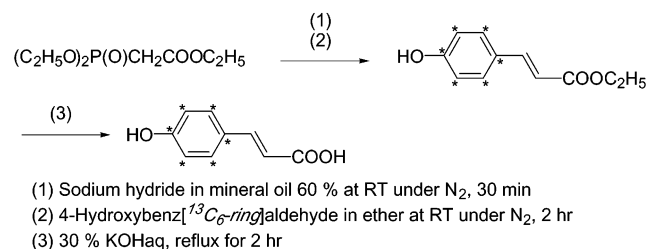
To understand the photocycle mechanism of PYP in atomic details, structural characterizations of the intermediate states are essential. Such information on the requisite time scales can be provided by resonance Raman spectroscopy, which can probe individual functional groups of proteins through their frequencies and intensities. In fact, this technique has played a key role in the study of the determination of the chromophore structure during the photocycle.^{8–11} However, a completely satisfactory framework for the interpretation of the observed spectra is not yet available because of a lack of a complete assignment of the chromophore vibrations.

Previous studies^{9,10} reported the high-frequency region of the resonance Raman spectra of PYP_M. Here we have obtained the spectra of PYP_M that contains the isotopically labeled chromophore in the 600–1700 cm⁻¹ region. We also present the results of normal mode calculations based on the density functional theory (DFT). These studies allow us to assign all of the observed Raman bands of PYP_M. The complete assign-

SCHEME 1: Preparation of 4-Hydroxycinnamic[9-¹³C₁] Acid



SCHEME 2: Preparation of 4-Hydroxycinnamic[1,2,3,4,5,6-¹³C₆] Acid



ment of the chromophore vibrations confirms that the chromophore of PYP_M in solution is in the cis configuration and its phenolic oxygen is protonated. Furthermore, the present normal mode calculations also have an important implication for the analysis of the Fourier transform infrared (FTIR) spectra of PYP. With assignments in hand, vibrational spectroscopy provides a unique approach for studying protein dynamic processes in PYP.

Materials and Methods

Preparation of ¹³C-Labeled Chromophores. ¹³C-labeled 4-hydroxycinnamic acids were prepared according to the method described previously¹² with its minor modification (Schemes 1 and 2).

The ¹³C-labeled reagents, triethylphosphonoacetate[¹³C₁] (Aldrich) and 4-hydroxybenz[¹³C₆]aldehyde (Cambridge Isotope Laboratory), were used and were commercially available. Under

* To whom correspondence should be addressed. E-mail: unno@tagen.tohoku.ac.jp or yamauchi@tagen.tohoku.ac.jp.

[†] Tohoku University.

[‡] Osaka University.

a nitrogen atmosphere, 4-hydroxybenzaldehyde was treated with phosphonate anion, which was generated from triethylphosphonoacetate at room temperature. After 4 h stirring, ethyl 4-hydroxycinnamate was obtained and then hydrolyzed in 30% potassium hydroxide. After usual workup and purification, colorless 4-hydroxycinnamic acid was obtained. The purity was checked with mass spectrometry and ^1H NMR spectroscopy.

Sample Preparations. Expression of wild-type PYP from *E. coli*, chromophore reconstitution, and protein purification were performed as described previously.¹³ ^{13}C -labeled PYPs were prepared by reconstitution of apo-protein with the above-mentioned 4-hydroxycinnamic anhydride whose carbonyl carbon atom (C9) or ring carbon atoms (C1–C6) were labeled with ^{13}C . These labeled samples are denoted as $^{13}\text{C}=\text{O}$ and $^{13}\text{C}_6$ -ring isotopomers, respectively. PYP in buffered D_2O (90% D_2O /10% H_2O) was prepared by proper dilution of a concentrated protein in 100 mM citrate/200 mM phosphate buffer at pH 5.0 into D_2O , and then the sample was incubated overnight at room temperature before the measurements. PYP in D_2O is designated as an O1-D isotopomer.

Resonance Raman Spectroscopy. Resonance Raman spectra were obtained as described previously.^{9,10} A liquid-nitrogen-cooled CCD detector (Instrument S. A., Inc.) recorded the Raman spectra after a Triax190 spectrometer (600 grooves/mm grating, 0.19 m focal length; Instrument S. A., Inc.) removed the excitation light, and a Spex 500M spectrometer (3600 grooves/mm grating, 0.5 m focal length) dispersed the scattered light. The 325.0 nm line from a helium–cadmium (IK5651R–G, Kimmon Electric Co., Ltd.) laser excited the samples at a 90° angle relative to the axis of the collection optics. A polarization scrambler is placed at the entrance of the spectrometer. The depolarization ratio is defined as the intensity of the scattered light observed with polarization perpendicular to the polarization of the excitation light divided by the intensity of the scattered light with polarization parallel to the incident light. The intensities of the Raman scattered light with polarization perpendicular and parallel to that of the incident light were measured using an ultra-violet sheet polarizer, which is placed in front of the polarization scrambler. PYP_M was produced as a photostationary state by continuous laser illumination at 441.6 nm during the measurement. Because the probe wavelength is only suited for the resonance enhancement of PYP_M ($\lambda_{\text{max}} = 355$ nm), interference from other photocycle intermediates is absent. The measurements were made on samples contained in a quartz spinning cell (10 mm in diameter). All spectra were taken at room temperature ($\sim 23^\circ\text{C}$), and a homemade software eliminated the noise spikes in the spectra caused by cosmic rays. The 100 μm slit width employed in these measurements corresponds to an instrumental resolution of ~ 4 cm^{-1} . All Raman spectra were calibrated using neat fenchone. The peak positions in the Raman spectra are measured by fitting the data with Gaussian line shapes on a polynomial background using a nonlinear least-squares fitting routine.

DFT Calculations. Among the numerous available DFT methods, we have selected the B3LYP hybrid functional with the 6-31G** basis set because of its high accuracy for predicting vibrational frequencies. It has been shown that this level of DFT calculations yield molecular force fields and vibrational frequencies in excellent agreement with experiments in a variety of systems.¹⁴ The optimized geometry, the harmonic vibrational frequencies, and Raman intensity were calculated using the DFT method mentioned above via the Gaussian 98 program.¹⁵ The calculated frequencies were scaled using a factor of 0.9613. We note that the experimental spectra are obtained under resonance condition, but the calculated nonresonance Raman intensities

represent a good approximation in our system. Indeed the nonresonance Raman spectra excited at 647.1 nm of PYP_{dark} and an acid-induced bleached state PYP_{M, dark} are very similar to those of their resonance Raman spectra (not shown).

Resonance Raman Spectra of Photodegradable Samples.

We consider a system that exhibits simple $\text{A} \rightarrow \text{B}$ photodecomposition with a rate constant k , where A and B stand for intact and decomposed species, respectively. Raman intensities at ν cm^{-1} for species A and B are defined as $I_A(\nu)$ and $I_B(\nu)$, respectively. Because the fraction of species A and B at time t is e^{-kt} and $1 - e^{-kt}$, respectively, the experimentally observed spectrum can be expressed by

$$I(\nu, t_0, t_1) = \int_{t_0}^{t_1} e^{-kt} I_A(\nu) + (1 - e^{-kt}) I_B(\nu) dt \quad (1)$$

where the spectrum is measured between t_0 and t_1 and the sample starts to expose to the laser light at $t = 0$. In a slow photodegradation limit, $kt \ll 1$, $e^{-kt} = 1 - kt$ and the observed spectrum $I(\nu, t_0, t_1)$ is evaluated as follows:

$$\begin{aligned} I(\nu, t_0, t_1) &\cong \int_{t_0}^{t_1} (1 - kt) I_A(\nu) + kt I_B(\nu) dt \\ &= \{t_1 - t_0 - 0.5k(t_1^2 - t_0^2)\} I_A(\nu) + \\ &\quad 0.5k(t_1^2 - t_0^2) I_B(\nu) \quad (2) \end{aligned}$$

If three spectra of $I(\nu, 0, \Delta t)$, $I(\nu, \Delta t, 2\Delta t)$, and $I(\nu, 2\Delta t, 3\Delta t)$ are sequentially acquired, we can calculate the following difference spectrum $\Delta I(\nu, \Delta t)$, which shows the spectral changes because of the sample decomposition:

$$\begin{aligned} \Delta I(\nu, \Delta t) &= I(\nu, \Delta t, 2\Delta t) - I(\nu, 0, \Delta t) = \\ &\quad I(\nu, 2\Delta t, 3\Delta t) - I(\nu, \Delta t, 2\Delta t) \\ &= k\Delta t^2 [I_B(\nu) - I_A(\nu)] \quad (3) \end{aligned}$$

Equation 3 indicates that the difference spectrum $\Delta I(\nu, \Delta t)$ does not change during the measurement. In this situation, the following equation is derived:

$$I_A(\nu) = \{I(\nu, 0, \Delta t) - 0.5\Delta I(\nu, \Delta t)\} / \Delta t \quad (4)$$

This implies that the resonance Raman spectrum of the intact species A can be obtained with eq 4, if the observed data satisfy eq 3.

Results and Discussion

1. Resonance Raman Spectrum of PYP_M. The time dependence of the resonance Raman spectrum of PYP_M is shown in Figure 1A, which illustrates the gradual changes of the prominent doublet near 1600 cm^{-1} . This is clearly seen in the difference spectra of $I(\nu, 7 \text{ min}, 14 \text{ min}) - I(\nu, 0 \text{ min}, 7 \text{ min})$ (trace d) and $I(\nu, 14 \text{ min}, 21 \text{ min}) - I(\nu, 7 \text{ min}, 14 \text{ min})$ (trace e). Traces d and e are essentially same, indicating that the present experimental condition fulfills eq 3. Thus, the observed spectrum can be corrected with eqs 3 and 4 to obtain the resonance Raman spectrum of intact PYP_M. We present the corrected spectra in the rest of this paper.

Figure 1B examines the resonance Raman spectra of PYP_M as a function of the power of the probe laser light (traces g–i). The figure also shows the spectrum of an acid-induced bleached state PYP_{M, dark} (trace f), which presumably contains protonated *trans*-chromophore.⁹ Although overall spectral features do not vary with different laser powers, there are some distinct differences in the spectrum as evident in the difference spectrum

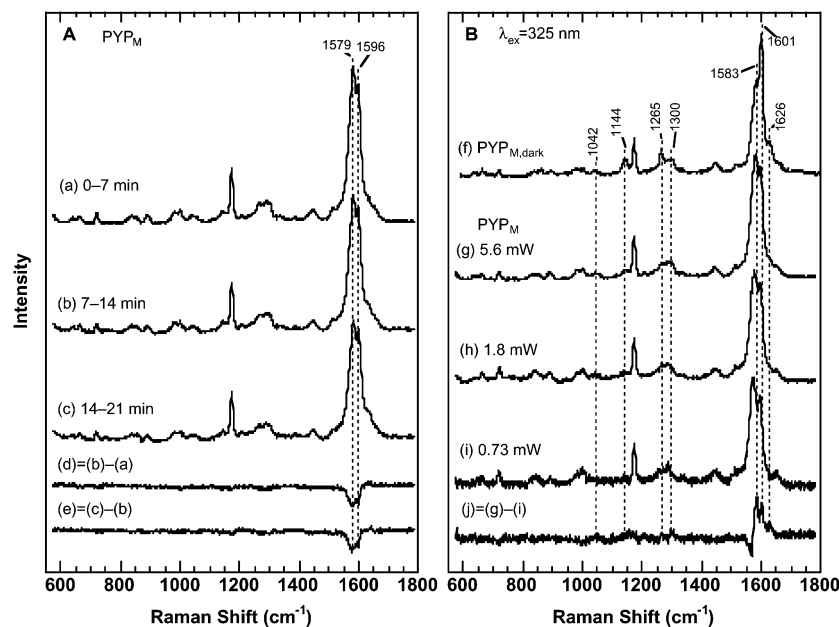


Figure 1. (A) Time dependence of the resonance Raman spectra of PYP_M in 10 mM citrate/20 mM phosphate buffer pH 5.0 at (a) 0–7, (b) 7–14, and (c) 14–21 min. The spectra were obtained with 325.0 nm excitation (5.6 mW) under continuous laser illumination at 441.6 nm (5.6 mW). The sample concentration was 100 μ M. Traces d and e are the difference spectra of spectra b minus a and spectra c minus b, respectively. (B) Resonance Raman spectra of PYP_{M,dark} and PYP_M. Trace f: For PYP_{M,dark}, the sample was dissolved in 20 mM citrate/HCl buffer at pH 2.0 with excitation at 325.0 nm (2.6 mW). Traces g–i: The laser power dependence of the resonance Raman spectra of PYP_M in 10 mM citrate/20 mM phosphate buffer at pH 5.0. The spectra were obtained at (g) 5.6, (h) 1.8, and (i) 0.73 mW of the 325.0 nm probe laser power. The pump laser power was 5.6 mW. Trace j is the difference spectrum recorded at high power (5.6 mW) minus that recorded at low power (0.73 mW) where the sharp Raman band at 1163 cm^{-1} balance out.

(trace j) between those with high (trace g) and low (trace i) laser powers. The most significant changes are seen at the main bands of $\sim 1600 \text{ cm}^{-1}$, and some minor bands appear around 1042, 1144, 1265, and 1300 cm^{-1} . These new features in the high power spectrum also exist in the spectrum of PYP_{M,dark}. Thus, we ascribe these Raman bands to a reversible photoproduct of PYP_M, whose chromophore is in trans configuration like PYP_{M,dark}. In this study, we have performed a set of experiments with the intermediate laser power (1.8 mW), where we can get moderate signal intensity and relatively small fraction of the photoproduct.

Figures 2 and 3 show the resonance Raman spectra of PYP_M in the low and high-frequency regions, respectively. We measured the spectrum of PYP_M in buffered D₂O solution, where the phenolic OH group of the chromophore is deuterated (trace b). The resonance Raman spectra are also shown for PYP whose chromophore is labeled with ¹³C at the carbonyl carbon atom (trace c) or at ring carbon atoms (trace d). In addition, the figure illustrates the H/D and ¹²C/¹³C difference spectra (traces e–g), where the effect of the isotopic substitutions can be clearly seen. The observed frequencies and isotope shifts are summarized in Table 1. To interpret these experimental results, we next perform normal mode calculations as described below.

2. Normal Mode Calculations Based on DFT. We have employed protonated *cis*-4-hydroxycinnamyl methyl thiolester (HCMT) as a chromophore model for normal mode calculations.^{9,10} For geometry optimization, the starting geometry was taken from the crystal structure of PYP_M,¹⁶ and the obtained structures are depicted in Figure 4. Table 1S (Supporting Information) gives the optimized geometries along with the experimental parameters of PYP_M in crystal.¹⁶ There are two possible conformations having different orientation of the phenolic OH group (models 1 and 2). In both cases, optimized geometry is C_s symmetry, whereas the crystal structure of PYP_M¹⁶ showed a highly distorted chromophore (Table 1S).

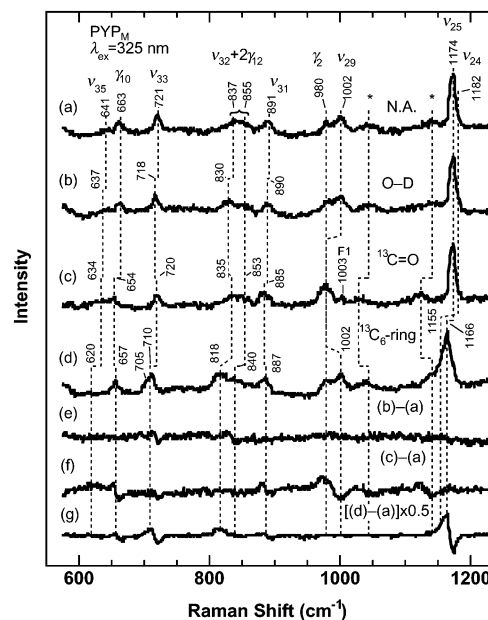


Figure 2. Low-frequency resonance Raman spectra of PYP_M and its isotopomers in 10 mM citrate/20 mM phosphate buffer pH 5.0. The spectra were obtained with 325.0 nm excitation (1.8 mW) under continuous laser illumination at 441.6 nm (5.6 mW). The spectra for (a) natural abundance, (b) O1–D, (c) ¹³C=O, and (d) ¹³C₆-ring samples are shown. The difference spectra of the isotope effects are also given as traces d–g.

Although the energy of model 1 is ca. 1.2 kJ mol⁻¹ higher than that of model 2, the optimized structures are similar to each other except for the phenolic OH moiety, e.g., the O1–C1–C2 bond angle for model 1 is 122.8°, whereas the corresponding angle for model 2 is 117.5°. Figure 4 also shows the optimized structure of protonated *cis*-HCMT whose carbonyl O2 forms a hydrogen bond with amide nitrogen of methylamine (model 3).

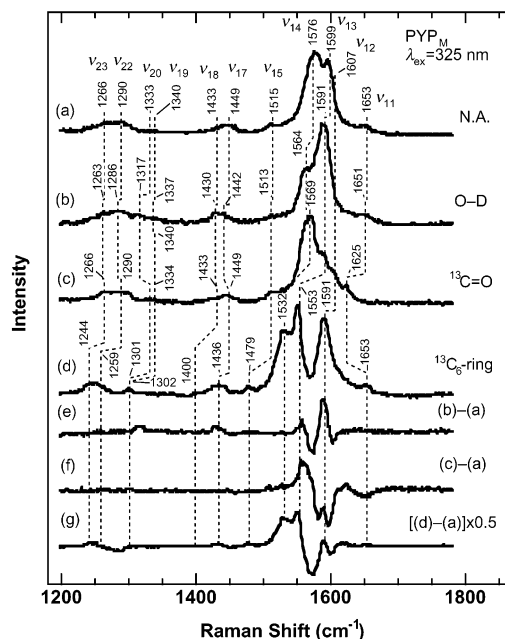


Figure 3. High-frequency resonance Raman spectra of PYP_M and its isotopomers. The experimental conditions and the samples are the same as those described in Figure 2.

A recent resonance Raman study demonstrates the presence of a hydrogen bond at carbonyl O2 for PYP_M in solution.¹⁰ As listed in Table 1S, the formation of the hydrogen bond mainly affects the carbonyl moiety of HCMT. For example, the C9–O2 bond distance increases by 0.007 Å, whereas the C9–S bond distance decreases by 0.019 Å upon formation of the hydrogen bond.

Next we have calculated vibrational frequencies as well as Raman intensities of protonated *cis*-HCMT using the optimized structures described above. On the basis of C_s symmetry, 63 fundamentals of protonated HCMT span the representation $\Gamma = 43 A' + 20 A''$ vibrations. All fundamental modes are Raman active, and A' and A'' type modes correspond to in-plane (ν_i) and out-of-plane (γ_i) vibrations, respectively. Figure 5 presents atomic displacements for selected normal modes of model 1. In addition to the observed frequencies, Table 1 summarizes the computed frequencies as well as approximate descriptions of the vibrational modes. The calculated isotope shifts for the O1–D, $^{13}\text{C}=\text{O}$, and $^{13}\text{C}_6$ -ring isotopomers are also shown in the table. For the O1–D isotopomer of model 3, two hydrogen atoms bound to the nitrogen atom of methylamine are also replaced by deuterium atoms, because the amide groups are expected to be deuterated in D_2O . Figures 6 and 7 illustrate the simulated Raman spectra of model 3 in four different isotopomers (traces a–d) as well as the H/D and $^{12}\text{C}/^{13}\text{C}$ difference spectra (traces e–g). Comparison of the observed (Figures 2 and 3) and calculated spectra demonstrates satisfactory agreements between the experiment and calculation, allowing us to assign all of the observed Raman bands of PYP_M. Because protonated HCMT contains 10 hydrogen atoms, ν_1 – ν_{10} correspond to the C–H or O–H stretching modes. Thus, we expect the remaining 53 normal modes in the 0–1700 cm^{-1} region. The details of the assignments will be given in the following section.

We note that, although the present DFT calculations reproduce main features of the observed spectra, there are some deviations from the experiment. For instance, the calculations nicely predict spectral features of the intense doublet near 1600 cm^{-1} (ν_{13} and ν_{14}) and its isotope shifts, but the differences between the

observed and calculated frequencies are somewhat large (Table 1). Further calculations including protein–chromophore interactions, such as steric and/or electrostatic effects of the protein moiety, may reduce the deviations. We should also note that the depolarization ratios of the observed Raman bands were nearly the same (~ 0.33). This implies that the observed spectra are truly resonantly enhanced with a nondegenerate excited state,¹⁶ and the depolarization ratio is not helpful for the assignment of the resonance Raman spectra of PYP_M.

3. Assignment. A. C=C or C=O Stretching Mode; ν_{11} – ν_{15} .

As depicted in Figure 3, the resonance Raman spectra from the natural abundance (trace a) and $^{13}\text{C}=\text{O}$ labeled (trace c) samples and their difference spectrum (trace f) confirm previous results,^{9,10} showing the Raman band at 1653 cm^{-1} for the C9=O2 stretching mode ν_{11} . The DFT calculations indicate that the ν_{11} frequency is sensitive to the presence or absence of a hydrogen bond at carbonyl O2, i.e., this mode undergoes a 28 cm^{-1} downshift in the presence of methylamine (model 1 \rightarrow 3). The observed frequency (1653 cm^{-1}) and the $^{13}\text{C}=\text{O}$ shift (-28 cm^{-1}) are consistent with the calculated values (1660 and -33 cm^{-1}) of model 3, indicating the presence of the hydrogen bond in PYP_M.¹⁰

The DFT calculations show that the 1550–1650 cm^{-1} region contains normal modes that are allocated to coupled C–C and C=C stretching modes of the aromatic ring and the ethylenic group (Figure 5). The intense Raman bands at 1599 and 1576 cm^{-1} have been assigned to ν_{13} and ν_{14} , respectively,^{9,10} which contain ring vibrations that correspond to Y8b of tyrosine.¹⁸ This assignment is confirmed by the $^{13}\text{C}_6$ -ring spectrum: these Raman bands exhibit a large shift of ca. -45 cm^{-1} upon $^{13}\text{C}_6$ -ring substitution (Figure 3), and similar isotope shifts are predicted by the calculations ($-39 \sim -47 \text{ cm}^{-1}$) (Figure 7). The strong ν_{13} band has a shoulder at 1607 cm^{-1} . We assign this band to ν_{12} , which can be related to Y8a of tyrosine.¹⁸ Although the ν_{12} band is not clear in the natural abundance sample (traces a and b in Figure 3), this mode clearly appears as a shoulder in the $^{13}\text{C}=\text{O}$ isotopomer (trace c) and even becomes a prominent Raman band at 1591 cm^{-1} for the $^{13}\text{C}_6$ -ring derivative (trace d). The simulated spectra shown in Figure 7 demonstrate the same trend. The shoulder at 1515 cm^{-1} is assigned to ν_{15} , coupled symmetric C–C stretching and C–H bending vibration of the phenolic ring (Figure 5), which is analogous to Y19a of tyrosine.¹⁸ This mode is seen at 1479 cm^{-1} in the $^{13}\text{C}_6$ -ring spectrum, and the observed 36 cm^{-1} downshift coincides with the calculated shift from 1496 to 1460 cm^{-1} for model 3.

B. C=C or C–C Stretching/C–H Rocking Modes; ν_{17} – ν_{23} .

The DFT calculations demonstrate that the normal modes in the 1200–1500 cm^{-1} region consist primarily of C=C or C–C stretching and in-plane C–H rocking vibrations (Figure 5, Table 1). The ν_{17} and ν_{18} modes of protonated *cis*-HCMT involve asymmetric stretching motions of the phenolic ring and HC7=C8H rocking motions (B_1 symmetry in local C_{2v}) with different phase. The observed bands at 1449 cm^{-1} and its shoulder at 1433 cm^{-1} are assigned to ν_{17} and ν_{18} , respectively (Figure 3). Because of different contributions of the ring C–C stretches, ν_{18} is expected to show a larger $^{13}\text{C}_6$ -ring shift (-29 cm^{-1}) compared to ν_{17} (-10 cm^{-1}). Such shifts of -33 (ν_{18}) and -13 cm^{-1} (ν_{17}) are observed in the $^{13}\text{C}_6$ -ring spectrum. Upon deuterium substitution of the phenolic OH group, the ν_{17} and ν_{18} modes are predicted to show $\sim 3 \text{ cm}^{-1}$ downshifts, which are experimentally observed ($-3 \sim -7 \text{ cm}^{-1}$).

The 1250–1350 cm^{-1} region has four normal modes (ν_{19} , ν_{20} , ν_{22} , and ν_{23}) that are combination of the aromatic ring and

TABLE 1: Observed and Calculated Vibrational Frequency (cm⁻¹) of PYP_M and Its Models^a

ν_{cal}^b model 1	ν_{cal}^b model 2	ν_{cal}^b model 3	ν_{obs}^c	assignment ^d
1688 (0, -38, -1)	1686 (0, -38, -1)	1660 (0, -33, -1)	1653 (-2, -28, 0)	ν_{11} $\nu\text{C9}=\text{O2}$
1608 (0, 0, -25)	1610 (-1, 0, -26)	1608 (0, 0, -27)	1605 (0, 0, -14)	ν_{12} $\nu\text{CC}(8a)$, $\nu\text{C7}=\text{C8}$
1583 (-4, -2, -41)	1576 (-1, -2, -39)	1582 (-4, -3, -40)	1599 (-8, -8, -46)	ν_{13} $\nu\text{C7}=\text{C8}$, $\nu\text{CC}(8b)$
1552 (-7, -2, -46)	1558 (-9, -2, -47)	1551 (-7, -4, -45)	1576 (-12, -7, -44)	ν_{14} $\nu\text{CC}(8b)$, $\nu\text{C7}=\text{C8}$
1496 (-1, 0, -36)	1499 (-2, 0, -36)	1496 (-1, 0, -36)	1515 (-2, -2, -36)	ν_{15} $\nu\text{CC}+\delta\text{CH}(19a)$
1433 (-3, -1, -10)	1433 (-3, -1, -9)	1433 (-3, -1, -10)	1449 (-7, 0, -13)	ν_{17} $\delta\text{HC7}=\text{C8H}(\text{B}_1)$, $\nu\text{CC}+\delta\text{CH}(19b)$
1416 (-4, -1, -29)	1412 (-3, -1, -30)	1416 (-4, -1, -29)	1433 (-3, 0, -33)	ν_{18} $\nu\text{CC}+\delta\text{CH}(19b)$, $\delta\text{HC7}=\text{C8H}(\text{B}_1)$
1342 (-8, 0, -26)	1338 (-3, 0, -32)	1342 (-8, 0, -32)	1340 (-3, 0, -38)	ν_{19} $\nu\text{CC}+\delta\text{CH}(3)$, $\delta\text{HC7}=\text{C8H}(\text{A}_1)$
1324 (-20, 0, -14)	1329 (-25, 0, -9)	1323 (-20, 0, -8)	1330 (-13, 0, -10)	ν_{20} $\nu\text{CC}+\delta\text{CH}(14)$, $\delta\text{HC7}=\text{C8H}(\text{A}_1)$
1274 (-4, 0, -30)	1274 (-6, 0, -27)	1273 (-4, 0, -30)	1290 (-4, 0, -31)	ν_{22} $\nu\text{C1}-\text{O1}(7a')$, $\delta\text{HC7}=\text{C8H}(\text{A}_1)$
1255 (-2, 0, -19)	1254 (0, 0, -21)	1254 (-2, 0, -19)	1266 (-3, 0, -22)	ν_{23} $\delta\text{HC7}=\text{C8H}(\text{A}_1)$
1171 (0, 0, -30)	1174 (-1, 0, -22)	1171 (0, 0, -30)	1182 (0, 0, -27)	ν_{24} $\nu\text{C4}-\text{C7}(7a)$
1163 (-1, 0, -4)	1165 (-4, 0, -4)	1163 (-1, 0, -4)	1174 (0, 0, -8)	ν_{25} $\delta\text{CH}(9a)$
1154 (-247, 0, -7)	1152 (-246, 0, -14)	1153 (-247, 0, -7)		ν_{26} δCOH
1100 (+4, 0, -14)	1097 (+5, -1, -15)	1099 (+4, 0, -14)		ν_{27} $\delta\text{CH}(15)$
991 (0, -1, -29)	991 (0, -1, -29)	990 (0, +2, -27)		ν_{28} $\nu\text{CC}+\delta\text{CCC}(18a)$
985 (0, -15, -1)	985 (+1, -15, -1)	1002 (0, -14, -2)	1002 (0, -23, 0)	ν_{29} $\nu\text{C8}-\text{C9}$
972 (0, 0, -1)	972 (0, 0, -1)	970 (0, -1, -1)	980 (+3, -1, +1)	γ_2 $\gamma\text{HC7}=\text{C8H}(\text{A}_2)$
969 (0, 0, -8)	955 (0, 0, -8)	968 (0, 0, -8)		γ_4 $\gamma\text{CH}(17a)$
903 (0, 0, -8)	922 (0, 0, -8)	903 (0, 0, -8)		γ_5 $\gamma\text{CH}(5)$
865 (-2, -7, -4)	865 (-2, -7, -4)	869 (-2, -5, -4)	891 (-1, -6, -6)	ν_{31} δC7C8C9
833 (0, 0, -11)	821 (0, 0, -12)	833 (0, 0, -11)		γ_6 $\gamma\text{CH}(11)$
820 (-5, -1, -23)	820 (-6, -1, -22)	820 (-6, -0, -23)	855 (0, -2, -15) ^e	$\nu_{32} +$ $\nu\text{CC}+\nu\text{CO}(1)$
2 × 421 (0, -1, -9)	2 × 419 (0, -1, -9)	2 × 421 (0, -1, -9)	837 (-7, -2, -19) ^e	2 × γ_{12} $\tau\text{CC}(16a)$
787 (0, 0, -7)	794 (-1, 0, -7)	788 (0, 0, -7)		γ_7 $\gamma\text{CH}(10a)$, $\gamma\text{C}_4\text{H}$
759 (0, -1, -5)	762 (-1, -1, -4)	760 (0, -2, -5)		γ_8 γC8H , $\gamma\text{CH}(10a)$
705 (-3, 0, -6)	706 (-3, 0, -7)	703 (-3, 0, -9)	721 (-3, -1, -9)	ν_{33} $\nu\text{CO}+\nu\text{CC}(13)$
703 (0, -4, -16)	703 (0, -4, -16)	705 (0, -4, -16)		γ_9 $\gamma\text{CO}+\gamma\text{CH}+\gamma\text{CC}(4)$, γC7H
692 (-1, 0, -4)	692 (-1, 0, -3)	686 (0, 0, -2)		ν_{34} $\gamma\text{S}-\text{C10}$
645 (0, -11, -6)	646 (0, -11, -6)	648 (0, -9, -6)	663 (0, -9, -6)	γ_{10} $\gamma\text{C9}=\text{O2}$, γC8H
637 (-2, -1, -20)	637 (-1, 0, -20)	637 (-2, -1, -19)	641 (0, -1, -21)	ν_{35} $\delta\text{CCC}(6b)$
571 (-1, -3, -7)	570 (0, -3, -6)	576 (-1, -3, -7)		ν_{36} δC4C7C8
507 (0, -1, -11)	507 (0, -1, -11)	507 (0, -1, -11)		γ_{11} $\gamma\text{CH}+\gamma\text{CO}+\gamma\text{CC}(16b)$

^a This table summarizes the observed and calculated frequencies in the 500–1700 cm⁻¹ region. Five normal modes that are localized in the methyl group of HCMT are not shown. ^b Calculated vibrational frequencies of protonated *cis*-HCMT. The numbers in parentheses are the isotope shifts of O1–D – na, ¹³C=O – na, and ¹³C₆-ring – na, respectively. na = natural abundance. ^c Observed vibrational frequencies of PYP_M. The numbers in parentheses are the isotope shifts of O1–D – na, ¹³C=O – na, and ¹³C₆-ring – na, respectively. The numbers in *italics* are not accurately determined. ^d The observed Raman bands are assigned to the calculated in-plane (ν_i) or out-of-plane (γ_i) normal modes of protonated *cis*-HCMT. Approximate descriptions of the calculated modes are also described. For ring vibrations, the corresponding vibrational modes of tyrosine are indicated. The (–HC7=C8H–) moiety of the chromophore can be approximately described by the point group C_{2v} for the two hydrogens, so that the local symmetry description is given for the hydrogen bending modes. ^e Fermi resonance that is analogous to the “tyrosine doublet”.

HC7=C8H (A₁) rocking motions. The ring vibration that is similar to Y3 of tyrosine contributes to ν_{19} , whereas ν_{20} contains Y14 like ring vibrations (Figure 5). We assign these modes to small shoulders around 1330 cm⁻¹ (Figure 3) and tentatively locate ν_{19} and ν_{20} at 1340 and 1330 cm⁻¹, respectively, on the basis of a fitting analysis. In contrast to the natural abundance spectrum, clear bands appear at 1317 and 1301 cm⁻¹ in the O1-D and ¹³C₆-ring spectra, respectively. The 1317 cm⁻¹ band of trace b is assigned to ν_{20} because of its large downshift (~25 cm⁻¹) upon the deuteration of the phenolic OH group (Table 1). The band at 1301 cm⁻¹ of trace d is assigned to ν_{19} , which shows a large downshift (~30 cm⁻¹) upon ¹³C₆-ring substitution (Table 1).

The ν_{22} and ν_{23} are coupled vibrations between the ring skeleton (Y7a') and the HC7=C8H rocking motions (Figure 5). We detected well-resolved spectral features at 1290 (ν_{22}) and 1266 (ν_{23}) cm⁻¹. These features shift down and collapse into a single broad band around 1245 cm⁻¹ for the ¹³C₆-ring spectrum. A fitting analysis estimates the ν_{22} and ν_{23} frequencies for the ¹³C₆-ring derivative at 1259 and 1244 cm⁻¹, respectively, leading to a larger downshift of ν_{22} (-31 cm⁻¹) compared to that of ν_{23} (-22 cm⁻¹). Similar downshifts of 31 and 19 cm⁻¹

are seen in the simulated spectra (Figure 7) for ν_{22} and ν_{23} , respectively.

C. Aromatic Ring Modes Containing C–H Rocking Motions; ν_{24} – ν_{28} . The 1000–1200 cm⁻¹ region contains normal modes that involve significant contributions of the ring C–H rocking motions. A sharp Raman band at 1174 cm⁻¹ has been assigned to ν_{25} , allocated to a Y9a type¹⁸ aromatic ring motions.¹⁰ This assignment is confirmed by a -8 cm⁻¹ ¹³C₆-ring shift (Figure 2), which corresponds to a -4 cm⁻¹ shift at 1163 cm⁻¹ for model 3 (Table 1). The present DFT calculations further predict a presence of ν_{24} slightly above (8 cm⁻¹) the intense ν_{25} band (Figure 6). Because ν_{24} is allocated to C4–C7 stretching coordinate (Y7a), a large isotopic shift of -30 cm⁻¹ is expected for the ¹³C₆-ring derivative. The ¹³C₆-ring spectrum of Figure 2 indeed shows a clear shoulder at 1155 cm⁻¹, which is assigned to ν_{24} of this isotopomer. We tentatively locate ν_{24} for the natural abundance sample at 1182 cm⁻¹ (8 cm⁻¹ above the ν_{25} band).

Three C–H rocking vibrations of the aromatic ring (ν_{26} , ν_{27} , and ν_{28}) locate in the 1000–1150 cm⁻¹ region (Table 1). Two broad bands at 1042 and 1144 cm⁻¹ are seen in Figure 3, but these are ascribed to a photoproduct of PYP_M as discussed

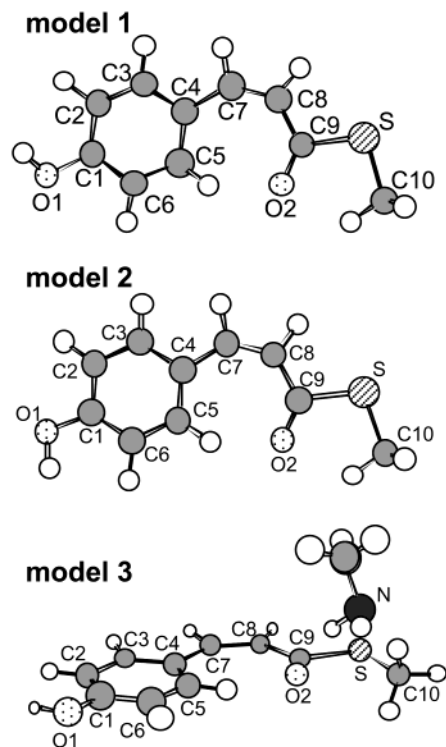


Figure 4. Optimized geometry of three models for protonated *cis*-4-hydroxycinnamyl methyl thiolester.

above. Thus, no candidates are found in the 325 nm excitation spectra of PYP_M for these modes.

D. Chromophore Skeleton Modes; ν_{29} – ν_{35} . Below the 1050 cm^{-1} region, normal modes of the chromophore skeleton appear (Figure 5). The ν_{29} mode involves a C8–C9 stretching motion and has been assigned to the band at 1002 cm^{-1} on the basis of its high sensitivity to $^{13}\text{C}=\text{O}$ substitution (Figures 2 and 6).¹⁰ This assignment is also supported by FTIR spectra of PYP_M; previous studies^{21,22,26,28} have found an IR band at $\sim 1000 \text{ cm}^{-1}$, which shows a sensitivity to C8–D isotopic substitution.²⁶ Note that the $^{13}\text{C}=\text{O}$ spectrum (trace c) of Figure 2 has a small band at 1003 cm^{-1} , which can be assigned to a ring-breathing vibration of phenylalanine residues denoted F1.¹⁹ In fact, a feature at 1003 cm^{-1} can be discerned on the relatively broad ν_{29} band for all spectra displayed in Figure 2.

The DFT calculations predict the in-plane C7=C8–C9 bending mode ν_{31} at 869 cm^{-1} for model 3 (Table 1, Figure 5). Because ring-breathing motions of the aromatic ring also contribute to ν_{31} , -5 and -4 cm^{-1} shifts are calculated for the $^{13}\text{C}=\text{O}$ and $^{13}\text{C}_6$ -ring isotopomers, respectively. This mode is assigned to a band at 891 cm^{-1} (Figure 2) on the basis of the observed -6 cm^{-1} shifts for $^{13}\text{C}=\text{O}$ and $^{13}\text{C}_6$ -ring substitutions.

A broad feature at $\sim 850 \text{ cm}^{-1}$ (Figure 2) can be assigned as a doublet at 837 and 855 cm^{-1} that arises from a Fermi resonance between the ring-breathing vibration ν_{32} and the overtone of an out-of-plane ring-bending vibration γ_{12} (Figure 5). Tyrosine residue exhibits a similar “tyrosine doublet” around 830–850 cm^{-1} .^{18,19} The present normal-mode analysis shows that deuteration of the phenolic OH group of the chromophore shifts down ν_{32} greatly (-23 cm^{-1}) compared to γ_{12} (-0.3 cm^{-1}). Thus, the separation between the ν_{32} and $2 \times \gamma_{12}$ frequencies becomes too large to cause the resonance interaction between the two energy levels effectively, and the removal of the Fermi resonance explains the D₂O-induced changes in the band shape of the doublet (traces a \rightarrow b in Figure 2). On the other hand, the calculated $^{13}\text{C}_6$ -ring shifts of ν_{32} (-19 cm^{-1})

and the overtone of γ_{12} ($-11 \times 2 = -22 \text{ cm}^{-1}$) are similar, accounting for the downshift of the whole doublet by $\sim 20 \text{ cm}^{-1}$ (traces a \rightarrow d).

Two skeleton vibrations (ν_{33} and ν_{34}) are expected to locate around 700 cm^{-1} (Figure 6). Although these modes mix together, ν_{33} (703 cm^{-1} for model 3) mainly includes O1–C1 and C4–C7 stretching coordinates such as Y13 of tyrosine,¹⁸ whereas the S–C10 stretching coordinate significantly contributes to ν_{34} (692 cm^{-1} for model 3). We assign the 721 cm^{-1} band to ν_{33} on the basis of its -3 cm^{-1} O1–D and -9 cm^{-1} $^{13}\text{C}_6$ -ring shifts (Table 1). On the other hand, there is no candidate for ν_{34} in the natural abundance spectrum in Figure 2. Note that, however, the ν_{33} band in the $^{13}\text{C}_6$ -ring spectrum has a clear shoulder at 705 cm^{-1} , which might correspond to ν_{34} .

The ring deformation mode ν_{35} , which is similar to Y6a of tyrosine,¹⁸ can be assigned to a broad feature at 641 cm^{-1} (Figure 2), because the observed frequency and a 21 cm^{-1} downshift for the $^{13}\text{C}_6$ -ring isotopomer are consistent with the calculation (637 cm^{-1} and -19 cm^{-1} shift for model 3).

E. Out-of-Plane Vibrational Modes; γ_2 and γ_{10} . There are 20 out-of-plane vibrational modes for the protonated *cis*-HCMT, and two of them are observed in PYP_M. The 980 cm^{-1} band is assigned to the A₂ type of HC7=C8H hydrogen out-of-plane wagging mode γ_2 (Figure 5) based on the calculated frequency of $\sim 970 \text{ cm}^{-1}$. This band is insensitive to all isotopic substitutions examined here (Figure 2 and Table 1). Although the lack of sensitivity is consistent with the assignment, a further study using a new isotopomer such as C7–D and/or C8–D is necessary for the firm assignment. Note that the assignment of γ_2 is consistent with the case of an 11-*cis*-retinal chromophore in rhodopsin, because similar A₂ type hydrogen out-of-plane mode has been detected at $\sim 970 \text{ cm}^{-1}$.²⁰

The calculated γ_{10} mode at 648 cm^{-1} for model 3 is mainly allocated to the C9=O2 wagging motion (Figure 5). The Raman band at 663 cm^{-1} is assigned to γ_{10} on the basis of the -9 cm^{-1} $^{13}\text{C}=\text{O}$ and -6 cm^{-1} $^{13}\text{C}_6$ -ring shifts, which coincide with the calculated shifts. The out-of-plane C–H wagging motions at the aromatic ring and ethylenic part mix into the C9=O2 wag, accounting for the sensitivity to $^{13}\text{C}_6$ -ring substitution.

4. Implication. A. Chromophore Structure. Previous studies^{9,10} have assigned some of the Raman bands of PYP_M such as ν_{11} , ν_{13} , ν_{14} , ν_{25} , and ν_{29} . These assignments are confirmed in the present study, which has the benefit of a new isotopomer $^{13}\text{C}_6$ -ring derivative. In addition, we have successfully assigned remaining Raman bands in the 600–1700 cm^{-1} region. The complete assignment of the resonance Raman spectrum allows us to unambiguously determine the chromophore structure of PYP_M in solution. We previously showed that the conversion of PYP_{dark} to PYP_M leads to significant changes in the spectrum.^{9,10} The most remarkable change is a $\sim 30 \text{ cm}^{-1}$ upshift of the ν_{13} band at 1558 cm^{-1} , and the ν_{13}/ν_{14} doublet appears at 1599 and 1576 cm^{-1} . The ν_{25} band also upshifts by 11 cm^{-1} from 1163 to 1174 cm^{-1} . These spectral changes have been ascribed to protonation of phenolic O1 in PYP_M.^{8–10} In this study, we have found that the deuteration effect on the $\nu_{32} + 2\gamma_{12}$ doublet around 850 cm^{-1} also acts as a marker for the protonation state of the chromophore (Figure 2). This is identical to the case of the “tyrosine doublet”, where the intensity ratio of the doublet is a measure of the protonation or the state of hydrogen bonding of the phenolic OH group.¹⁹ The ν_{33} band at 721 cm^{-1} also exhibits sensitivity toward O1–D substitution (Figure 2, Table 1) because of an involvement of

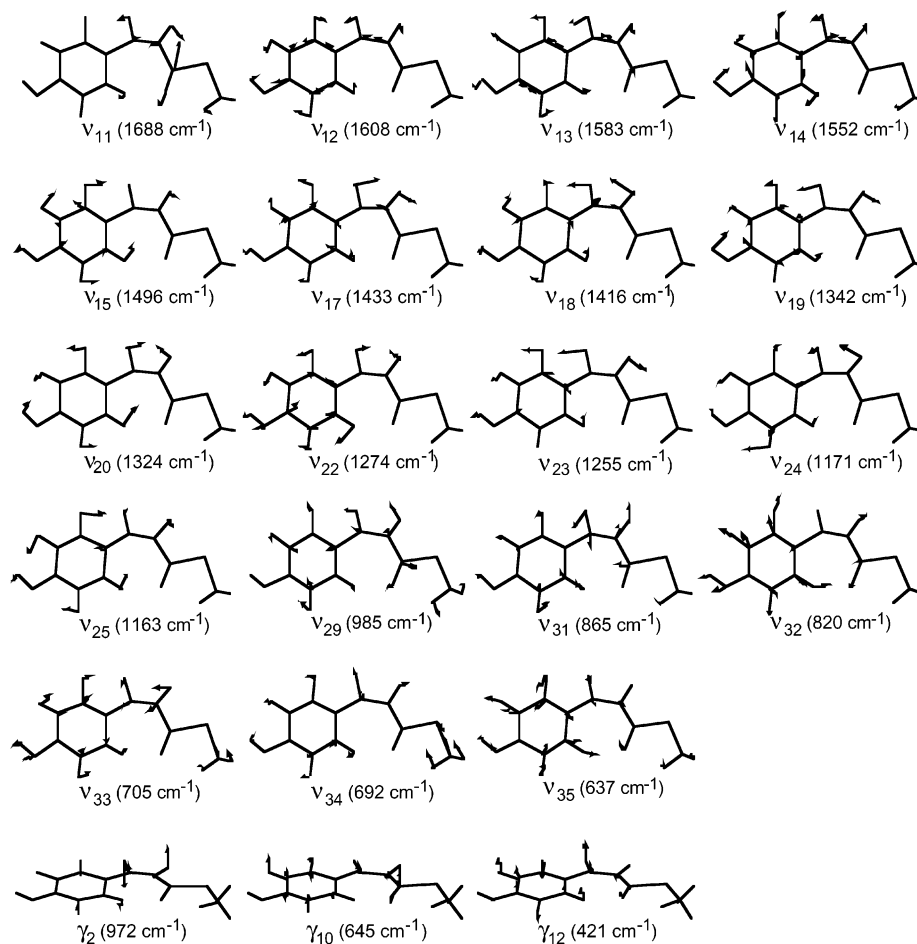


Figure 5. Atomic displacement vectors for some vibrational modes of protonated *cis*-4-hydroxycinnamyl methyl thiolester (model 1 in Figure 4).

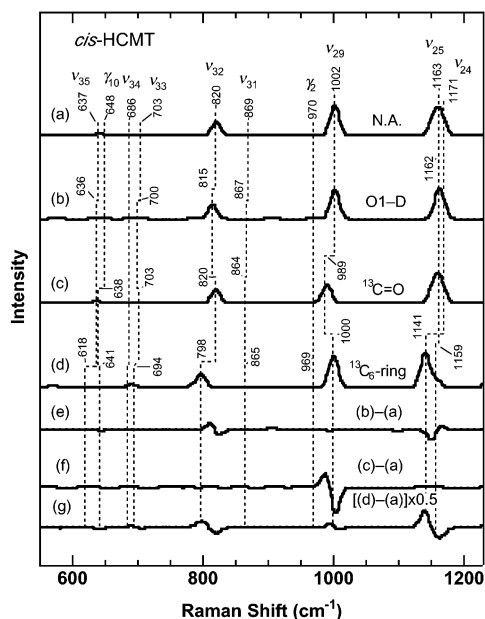


Figure 6. Simulated Raman spectra in the low-frequency region of protonated *cis*-4-hydroxycinnamyl methyl thiolester (model 3 in Figure 4). Gaussian band shapes with a 10 cm^{-1} width are used. The spectra for (a) natural abundance and (b) O1-D, (c) $^{13}\text{C}=\text{O}$, and (d) $^{13}\text{C}_6\text{-ring}$ isotopomers are shown. The difference spectra of the isotope effects are also given as traces d-g.

O1-C1 stretching coordinate (Figure 5). The latter observation provides further evidence for a protonated chromophore in PYP_M.

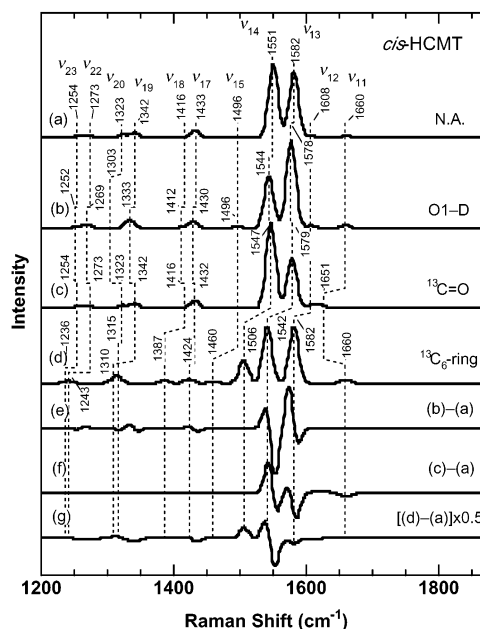


Figure 7. Simulated Raman spectra in the high-frequency region of protonated *cis*-4-hydroxycinnamyl methyl thiolester (model 3 in Figure 4). Gaussian band shapes with a 10 cm^{-1} width are used.

The observation of intense Raman bands (ν_{13} , ν_{14}) near 1600 cm^{-1} , which are associated with vibrations along the carbon-carbon double bond, is consistent with other cases such as bacteriorhodopsin.^{21,22} The frequency of the C=C stretching modes has been correlated with the extent of π -electron

delocalization of the retinal chromophore.²¹ In the case of PYP, the frequency of ν_{13} and ν_{14} for PYP_M and PYP_{M,dark}⁹ (1575–1600 cm⁻¹) is significantly higher than that for PYP_{dark} and PYP_L (~1555 cm⁻¹),^{9,10} indicating a less delocalized electronic structure that raises the C=C bond strength in PYP_M and PYP_{M,dark}.

As illustrated in Figure 4, there are two stable orientations of the phenolic OH group of the chromophore (models 1 and 2). The computed vibrational frequencies for these conformations are similar except for the intense ν_{13}/ν_{14} doublet near 1600 cm⁻¹. The splitting of the doublet is 31 cm⁻¹ for model 1 and 18 cm⁻¹ for model 2 (Table 1). The resonance Raman spectrum of PYP_M shows an intermediate splitting of 23 cm⁻¹. This observation may indicate that the chromophore in PYP_M has two configurations such as models 1 and 2. Such a disordered structure is consistent with recent findings that the formation of PYP_M possesses global conformational changes in the protein.^{23–29}

B. Implication for FTIR Studies. A recent FTIR study³⁰ on PYP suggested that the vibrational mode around 1300 cm⁻¹ is an indicator of the trans/cis isomerization of the chromophore. Free *trans*-4-hydroxycinnamic acid exhibits an IR band at 1294 cm⁻¹, whereas this band shifts down to 1288 cm⁻¹ upon photoisomerization. From the analogy to 4-hydroxycinnamic acid, a pair of bands at 1302/1286 cm⁻¹ in the PYP_{dark}/PYP_M difference IR spectrum was ascribed to the trans → cis isomerization of the chromophore. However, the present study shows that all vibrational modes around 1300 cm⁻¹ (ν_{19} – ν_{23}) are mainly allocated to the aromatic ring motions, implying a lack of sensitivity to the structural changes around the C7=C8 bond. Our assignment is also consistent with the available FTIR data for isotopically labeled PYP. Imamoto et al.³⁰ showed that the features around 1300 cm⁻¹ for the difference FTIR spectra are sensitive to deuterium labeling of the aromatic ring (C2-D/C6-D) but insensitive to that of the ethylenic bond (C8-D). Thus, the IR band at 1302 cm⁻¹ can be assigned to the phenolic ring stretching and C–H rocking mode ν_{20} of PYP_{dark},³¹ and the feature at 1286 cm⁻¹ is tentatively assigned to ν_{22} (1290 cm⁻¹) of PYP_M.

We previously showed that the C8–C9 stretching mode ν_{29} acts as a marker for trans/cis isomerization of the chromophore.¹⁰ The *trans* configuration exhibits the ν_{29} band at ~1050 cm⁻¹, whereas ν_{29} for the *cis* form is 990–1000 cm⁻¹. In the resonance Raman spectrum, ν_{29} of PYP_{dark} is observed as a doublet at 1042 and 1057 cm⁻¹, and it appears as a singlet at 1054 cm⁻¹ for PYP_{dark} in D₂O.^{8–10} Previous FTIR studies^{24–26,30,32} showed a corresponding doublet near 1050 cm⁻¹ for PYP_{dark}, and this feature is found to be highly sensitive to the C8-D isotopic substitution.³⁰ Furthermore, the deuterated PYP sample shows a singlet band at 1056 cm⁻¹,³⁰ indicating that the IR feature at ~1050 cm⁻¹ can be assigned to ν_{29} of PYP_{dark}. The time-resolved FTIR study²⁶ has found a band at 1003 cm⁻¹ for PYP_M in solutions, and similar band was observed at 994 cm⁻¹ for the frozen sample.^{25,30,32} This band is moderately sensitive to C8-D isotopic substitution³⁰ and assigned to ν_{29} of PYP_M. The retinal proteins exhibit some Raman bands around 1200 cm⁻¹,^{21,22} and these modes are mixtures of C–C stretching and C–H in-plane bending motions such as ν_{29} of PYP. Because their pattern of frequencies and intensities is very sensitive to the configuration and conformation, they are called “fingerprint modes” of a retinal chromophore. Thus, the ν_{29} mode can be designated as a fingerprint mode of a 4-hydroxycinnamyl chromophore and is useful for both resonance Raman and FTIR investigations of PYP.

In conclusion, this study presents the resonance Raman investigation of PYP_M in solution at room temperature. We have examined the effects of isotopic substitutions of the chromophore, and all of the observed Raman bands are assigned with the aid of DFT calculations. With these assignments in hand, resonance Raman spectroscopy provides an important approach for studying the photocycle mechanism in PYP. Further studies using time-resolved resonance Raman spectroscopy as well as complete vibrational assignments of PYP_{dark} and PYP_L are currently in progress.

Acknowledgment. We are grateful to N. Hamada (Osaka University) for helpful discussion and K. Yoshihara (Suntory Institute for Bioorganic Research) for assistance in preparing the ¹³C-labeled compounds. This work was supported by grants from the Naito Foundation to M.U. and by Grant-in-Aids No. 10780399 (M.U.) and No. 10044057 (S.Y.) from the Ministry of Education, Culture, Science, Sports, and Technology of Japan.

Supporting Information Available: The table that shows the optimized geometries along with the experimental parameters of PYP_M in crystal. This material is available free of charge via the Internet at <http://pubs.acs.org>.

References and Notes

- (1) Meyer, T. E. *Biochim. Biophys. Acta* **1985**, *806*, 175–183.
- (2) Hoff, W. D.; Dux, P.; Devreese, B.; Roodzant-Nugteren, I. M.; Crielgaard, W.; Boelens, R.; Kaptein, R.; Van Beeumen, J.; Hellingwerf, K. *J. Biochemistry* **1994**, *33*, 13959–13962.
- (3) Baca, M.; Borgstahl, G. E. O.; Boissinot, M.; Burke, P. M.; Williams, D. R.; Slater, K. A.; Getzoff, E. D. *Biochemistry* **1994**, *33*, 14369–14377.
- (4) Hoff, W. D.; van Stokkum, I. H. M.; van Ramesdonk, H. J.; van Brederode, M. E.; Brouwer, A. M.; Fitch, J. C.; Meyer, T. E.; van Grondelle, R.; Hellingwerf, K. *J. Biophys. J.* **1994**, *67*, 1691–1705.
- (5) Imamoto, Y.; Kataoka, M.; Tokunaga, F. *Biochemistry* **1996**, *35*, 14047–14053.
- (6) Ujj, L.; Devanathan, S.; Meyer, T. E.; Cusanovich, M. A.; Tollin, G.; Atkinson, G. H. *Biophys. J.* **1998**, *75*, 406–412.
- (7) Takeshita, K.; Imamoto, Y.; Kataoka, M.; Tokunaga, F.; Terajima, M. *Biochemistry* **2002**, *41*, 3037–3048.
- (8) Kim, M.; Mathies, R. A.; Hoff, W. D.; Hellingwerf, K. *J. Biochemistry* **1995**, *34*, 12669–12672.
- (9) Unno, M.; Kumauchi, M.; Sasaki, J.; Tokunaga, F.; Yamauchi, S. *J. Am. Chem. Soc.* **2000**, *122*, 4233–4234.
- (10) Unno, M.; Kumauchi, M.; Sasaki, J.; Tokunaga, F.; Yamauchi, S. *Biochemistry* **2002**, *41*, 5668–5674.
- (11) Zhou, Y.; Ujj, L.; Meyer, T. E.; Cusanovich, M. A.; Atkinson, G. H. *J. Phys. Chem. A* **2001**, *105*, 5719–5726.
- (12) William, S. W., Jr.; William, D. E. *J. Am. Chem. Soc.* **1961**, *83*, 1733–1738.
- (13) Imamoto, Y.; Ito, T.; Kataoka, M.; Tokunaga, F. *FEBS Lett.* **1995**, *374*, 157–160.
- (14) Koch, W.; Holthausen, M. C. *A Chemist's Guide to Density Functional Theory*; Wiley-VCH: Weinheim, Germany, 2000.
- (15) Frisch, M. J.; Trucks, G. W.; Schlegel, H. B.; Scuseria, G. E.; Robb, M. A.; Cheeseman, J. R.; Zakrzewski, V. G.; Montgomery, J. A., Jr.; Stratmann, R. E.; Burant, J. C.; Dapprich, S.; Millam, J. M.; Daniels, A. D.; Kudin, K. N.; Strain, M. C.; Farkas, O.; Tomasi, J.; Barone, V.; Cossi, M.; Cammi, R.; Mennucci, B.; Pomelli, C.; Adamo, C.; Clifford, S.; Ochterski, J.; Petersson, G. A.; Ayala, P. Y.; Cui, Q.; Morokuma, K.; Malick, D. K.; Rabuck, A. D.; Raghavachari, K.; Foresman, J. B.; Cioslowski, J.; Ortiz, J. V.; Stefanov, B. B.; Liu, G.; Liashenko, A.; Piskorz, P.; Komaromi, I.; Gomperts, R.; Martin, R. L.; Fox, D. J.; Keith, T.; Al-Laham, M. A.; Peng, C. Y.; Nanayakkara, A.; Gonzalez, C.; Challacombe, M.; Gill, P. M. W.; Johnson, B. G.; Chen, W.; Wong, M. W.; Andres, J. L.; Head-Gordon, M.; Replogle, E. S.; Pople, J. A. *Gaussian 98*; Gaussian, Inc.: Pittsburgh, PA, 1998.
- (16) Genick, U. K.; Borgstahl, G. E. O.; Ng, K.; Ren, Z.; Pradervand, C.; Burke, P. M.; Srajer, V.; Teng, T.-Y.; Schildkamp, W.; McRee, D. E.; Moffat, K.; Getzoff, E. D. *Science* **1997**, *275*, 1471–1475.
- (17) Strommen, D. S. *J. Chem. Educ.* **1992**, *69*, 803–807.
- (18) Takeuchi, H.; Watanabe, N.; Harada, I. *Spectrochim. Acta* **1988**, *44A*, 749–761.

- (19) Harada, I.; Takeuchi, H. In *Spectroscopy of Biological Systems*; Clark, R. J. H., Hester, R. E., Eds.; John Wiley & Sons: Chichester, U.K., 1981; Vol. 13, chapter 3.
- (20) Eyring, G.; Curry, B.; Broek, A.; Lugtenburg, J.; Mathies, R. *Biochemistry* **1982**, *21*, 384–393.
- (21) Stockburger, M.; Alshuth, T.; Oesterheld, D.; Gärtner, W. In *Spectroscopy of Biological Systems*; Clark, R. J. H., Hester, R. E., Eds.; John Wiley & Sons: Chichester, U.K., 1986; pp 483–535.
- (22) Mathies, R. A.; Smith, S. O.; Palings, I. In *Biological Applications of Raman Spectroscopy Vol II*; Spiro, T. G., Ed.; Wiley-Interscience: New York, 1988; pp 59–108.
- (23) Rubinstenn, G.; Vuister, G. W.; Mulder, F. A. A.; Düx, P. E.; Boelens, R.; Hellingwerf, K. J.; Kaptein, R. *Nat. Struct. Biol.* **1998**, *5*, 568–570.
- (24) Hoff, W. D.; Xie, A.; Van Stokkum, I. H. M.; Tang, X.; Gural, J.; Kroon, A. R.; Hellingwerf, K. J. *Biochemistry* **1999**, *38*, 1009–1017.
- (25) Kandori, H.; Iwata, T.; Hendriks, J.; Maeda, A.; Hellingwerf, K. J. *Biochemistry* **2000**, *39*, 7902–7909.
- (26) Brudler, R.; Rammelsberg, R.; Woo, T. T.; Getzoff, E. D.; Gerwert, K. *Nat. Struct. Biol.* **2001**, *8*, 265–270.
- (27) Xie, A.; Kelemen, L.; Hendriks, J.; White, B. J.; Hellingwerf, K. J.; Hoff, W. D. *Biochemistry* **2001**, *40*, 1510–1517.
- (28) Shiozawa, M.; Yoda, M.; Kamiya, N.; Asakawa, N.; Higo, J.; Inoue, Y.; Sakurai, M. *J. Am. Chem. Soc.* **2001**, *123*, 7445–7446.
- (29) Sasaki, J.; Kumauchi, M.; Hamada, N.; Oka, T.; Tokunaga, F. *Biochemistry* **2002**, *41*, 1915–1922.
- (30) Imamoto, Y.; Shirahige, Y.; Tokunaga, F.; Kinoshita, T.; Yoshihara, K.; Kataoka, M. *Biochemistry* **2001**, *40*, 8997–9004.
- (31) To be submitted for publication.
- (32) Imamoto, Y.; Mihara, K.; Hisatomi, O.; Kataoka, M.; Tokunaga, F.; Bojkova, N.; Yoshihara, K. *J. Biol. Chem.* **1997**, *272*, 12905–12908.